Journal of
Nanotheranostics

MDPI

Article

Nano-Enabled Colorimetric Assay for the Detection of *Paracoccidioides lutzii*: Advancing Diagnostics with Nanotechnology

Olavo O. Comparato Filho [1], Marcela A. Cândido [1], Aveline Ventura [1], Flavia V. Morais [2] and Leandro Raniero [1,*]

[1] Nanosensors Laboratory, Research & Development Institute, University of Vale do Paraíba, Av. Shishima Hifumi, 2911, Urbanova, São José dos Campos 12244-000, São Paulo, Brazil; comparatofilho@gmail.com (O.O.C.F.); marcela.aparecida.candido@gmail.com (M.A.C.); aveline.ventura@hotmail.com (A.V.)
[2] Cellular and Molecular Biology of Fungi Laboratory, Research & Development Institute, University of Vale do Paraíba, Av. Shishima Hifumi, 2911, Urbanova, São José dos Campos 12244-000, São Paulo, Brazil; flavia@univap.br
* Correspondence: lraniero@univap.br; Tel.: +55-12-3947-1132

Abstract: Deforestation is a common occurrence driven by agricultural expansion, urbanization, and infrastructure development. These activities often lead to increased human interaction with ecosystems, potentially exposing individuals to Paracoccidioides spores (*P. brasiliensis* and *P. lutzii*) found in the soil, resulting in Paracoccidioidomycosis (PCM). This fungal infection is endemic to specific regions in Latin America, such as Brazil, Colombia, Venezuela, and Argentina. Diagnosis typically involves a combination of clinical assessment, imaging techniques, and laboratory examinations. *P. lutzii* lacks the glycoprotein Gp43, a key antigenic protein utilized in serological tests for PCM diagnosis. In this study, a colorimetric test employing gold nanoparticles (AuNPs) and label-free methodology was employed for *P. lutzii* detection. The effectiveness of the label-free colorimetric test was assessed using a total of 100 samples. This detection was achieved through the amplification of the gp43 gene and the use of a specific probe (5′CAGGGGTGCG3′) in conjunction with AuNPs. The receiver operating characteristic curve was employed to assess the test, revealing that the method can accurately detect *P. lutzii* with a sensitivity of 100% and a specificity of 100%. The findings indicate a substantial impact on remote endemic regions attributable to the implementation of cost-effective diagnostic methodologies.

Keywords: Paracoccidioidomycosis; *P. lutzii*; label-free

Citation: Filho, O.O.C.; Cândido, M.A.; Ventura, A.; Morais, F.V.; Raniero, L. Nano-Enabled Colorimetric Assay for the Detection of *Paracoccidioides lutzii*: Advancing Diagnostics with Nanotechnology. *J. Nanotheranostics* **2024**, *5*, 75–83. https://doi.org/10.3390/jnt5030005

Academic Editor: Seyed Moein Moghimi

Received: 28 May 2024
Revised: 21 June 2024
Accepted: 24 June 2024
Published: 26 June 2024

1. Introduction

Paracoccidioidomycosis is a systemic mycosis caused by a fungus called Paracoccidioides (P.), which can affect both humans and animals. Paracoccidioides ssp. infection primarily affects individuals engaged in soil management activities in endemic regions, including gardening, agriculture, rural labor, soil preparation, and deforestation work. [1]. Initially, *P. brasiliensis* was the only species of the genus, with numerous isolates exhibiting varying virulence behaviors [2], Gp43 isoforms [3], clinical manifestations [4,5], and genetic polymorphisms [6–9]. In 2014, *P. lutzii* was identified as a distinct species [10]. Recently, molecular studies have elucidated a genus containing seven species: *P. brasiliensis sensu stricto*, *P. lutzii*, *P. restrepiensis*, *P. americana*, *P. loboi*, *P. venezuelensis*, and *P. cetii*. However, *P. brasiliensis sensu stricto* is the most widely distributed species in Brazil, except in the Brazilian Midwest, where *P. lutzii* is dominant, and in the Brazilian Amazon Forest, where *P. loboi* is predominantly found [11–13]. All this diversity makes diagnosing PCM difficult in some regions of the country [14–16]. Mycological examination of fresh biopsied tissue is

usually used to make the diagnosis. This is mainly based on the serological diagnosis of the immunodominant antigen (Gp43, a 43 kDa glycoprotein), which is the main protein released by the fungal yeast form [17]. Additionally, histopathological and molecular diagnosis may be considered for a final decision [18]. Furthermore, clinical symptoms such as lung involvement can, in some cases, lead to clinical manifestations and radiological changes similar to those of tuberculosis [19–21]. *P. lutzii* has an active glucanase (Plp43) with partial antigenic activity against *P. brasiliensis*, Gp43 [22]. Gegembauer and coworkers demonstrated that *P. brasiliensis* exoantigens failed to recognize sera from Midwest patients, while *P. lutzii* exoantigens recognized the same sera 100% of the time. This indicates the need for a differential diagnosis for these species, given their poor sensitivity of 17.65% and 100% specificity [23].

In this study, a colorimetric test utilizing gold nanoparticles (AuNPs) and a label-free methodology was employed to detect *P. lutzii*. The label-free colorimetric test's effectiveness is based on standard polymerase chain reaction (PCR) results, which include a specific primer for *P. lutzii* as well as a probe with an oligonucleotide sequence present in this amplified region. The test colorimetric results are based on the optical properties of AuNPs, which change the localized surface plasmon resonance (LSPR) due to aggregation [24–26].

2. Materials and Methods

2.1. Nanoparticle Synthesis and Characterization

AuNPs were synthesized by the citrate reduction method described by Turkevich et al. [27]. The concentration of colloidal solution was determined by the Lambert–Beer law, assuming an extinction coefficient for the plasmon resonance of 4.7×10^4 M^{-1} cm^{-1}, which can be used for nanoparticles smaller than 85 nm [28]. The morphology was determined using transmission electron microscopy (TEM) with a FEI Titan Microscope (FEI Technologies Inc., Hillsboro, OR, USA), operating at 300 kV in parallel mode. To prepare the samples, a drop (~15 µL) of the AuNPs suspension was deposited on the TEM grid and allowed to dry at room temperature. The hydrodynamic diameter was measured by dynamic light scattering (DLS) using a Zetasizer Nano ZS90 from Malvern Instruments (Malvern Instruments Limited, Worcestershine, UK). In this analysis, 200 µL of AuNPs was added to a cuvette (ref. 67.758, Sarstedt), and measurements were carried out at 21 °C. The UV–visible spectra were collected by a spectrophotometer (NanoDrop, Thermo Scientific, ND-1000, Wilmington, DE, USA), which holds the samples by their natural surface tension properties without the need for a curvette. For all experiments, AuNPs were measured at a synthesized concentration of 7.8×10^{11} particles per mL.

2.2. Paracoccidioide lutzii DNA Extraction

The yeast form of *P. lutzii* was grown on the solid medium YPD (1% yeast extract, 2% peptone, and 2% dextrose) at 37 °C. DNA extraction from cultures was conducted using the methodology outlined by Cano et al. [29]. Approximately 10 mL of moist *P. lutzii* cells was ground to a fine powder using a mortar and pestle in a liquid nitrogen bath. This powder was combined with a 25 mL solution containing 50 mM Tris, 100 mM EDTA, 5% sarcosyl, and proteinase K. Subsequently, the resulting mixture was homogenized (by vortex mixer) for a duration of 10 min, followed by an incubation period of 2 h at 56 °C. After centrifugation, the DNA in the supernatant was purified through at least two extractions using a phenol–chloroform–isoamyl alcohol solution with a ratio of 50:49:1.

The primer oligonucleotides for the gp43 gene-specific amplification reaction to molecularly detect *P. lutzii* were designed using the National Center for Biotechnology Information database. The polymerase chain reaction (PCR) used the "forward" primer 5′ ACC AAG TCT TCG ATG AT 3′ and the "reverse" primer 5′ TAG ACC TCG CAC A 3′ to describe the amplified fragment, which corresponds to a conservative region present in different isolates of *P. lutzii*. Between these two sequences, we also selected a probe described by 5′ CAG GGG TGC G 3′ (Sigma-Aldrich™, Taufkirchen, Germany) for testing purposes.

For the PCR amplification, a total of 4 µL of *P. lutzii* DNA at a concentration of 200 ng/mL, 2 µL of each primer at a concentration of 10 mmol L^{-1}, and 45 µL of PCR Supermix (Invitrogen™, Carlsbad, CA, USA) were used with the following thermocycle: 1 cycle at 95 °C (5 min), 35 cycles at 95 °C (1 min), 40 °C (3 min), and 72 °C (2 min), followed by a final extension at 72 °C (5 min) and at 4 °C (5 min). The quantified DNA product was analyzed by a spectrophotometer (NanoDrop, Thermo Scientific, ND-1000, Wilmington, DE, USA) and agarose gel electrophoresis.

2.3. Colorimetric Tests Using Gold Nanoparticles and Data Processing

The assays were created by mixing 2 µL of the amplified "probe" sequence fragment at a concentration of 10 µmol L^{-1} with 5 µL of AuNPs at a concentration of 4×10^{-9} mol L^{-1}. For the positive test, 2 µL of the complementary fragment was added, while for the negative test, 2 µL of the non-complementary fragment was added. The tests underwent a temperature cycle consisting of 95 °C for 5 min, 50 °C for 10 min, and 25 °C for 10 s. Following this cycle, 1 µL of an aqueous solution of $MgCl_2$ at a concentration of 2.6 mmol L^{-1} was added. The average observation time for the reactions after the addition of the saline solution was 8 min. Fifty pairs of tests were conducted, and the results were analyzed using UV–visible spectroscopy, allowing for the development of a graphical method of analysis by areas under the spectral curves as well as by the receiver operating characteristic (ROC) curve. The analysis of the quality of positive and negative tests (R) and spectra, in both cases, could be initially verified through a mathematical technique using logarithmic calculations of areas. In this analysis, positive and negative tests were classified using Equation (1):

$$R = Ln(\propto) \quad (1)$$

where $\propto$ is the ratio of integrated areas between the spectral regions 488–530 nm and 533–575 nm, respectively.

3. Results

Figure 1 depicts the morphology of bared gold nanoparticles (AuNPs) through a transmission electron microscopy (TEM) micrograph. Additionally, it includes the UV–visible spectrum, size distribution, and zeta potential measured using DLS.

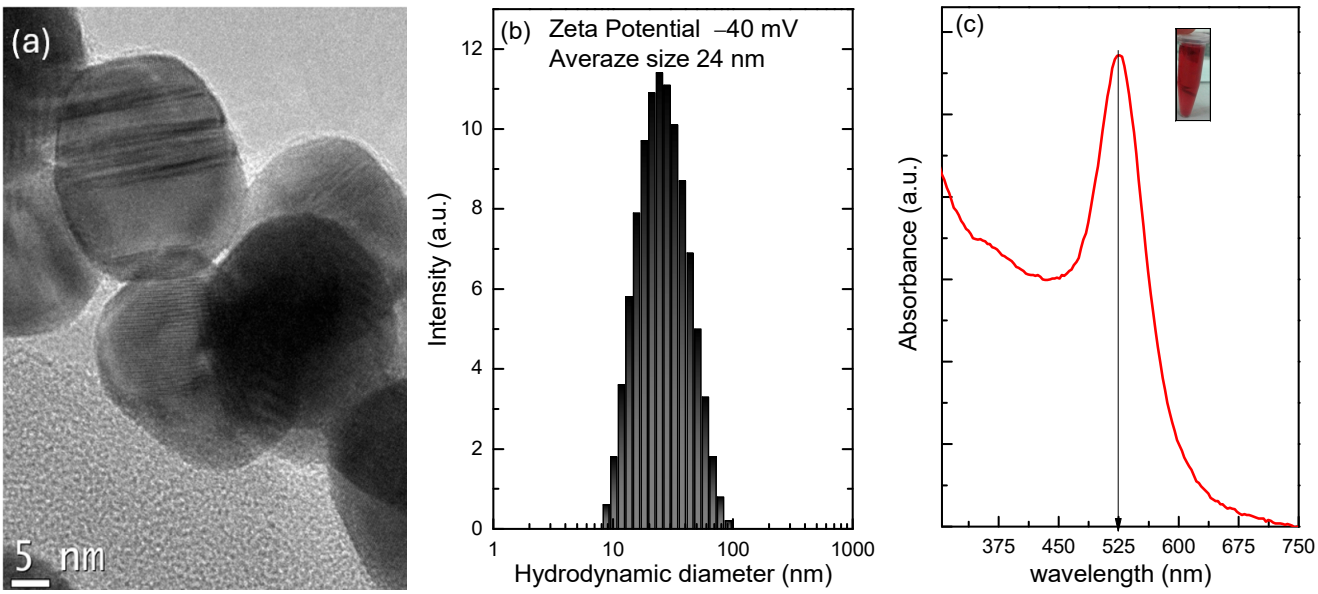

Figure 1. Gold nanoparticle characterization: (**a**) morphology by TEM; (**b**) hydrodynamic size distribution and zeta potential value; (**c**) UV–visible spectrum.

Figure 2 shows the results of the colorimetric test for detecting *P. lutzii*. In these tests, the DNA is isolated and amplified using a designated primer for *P. lutzii*. The test operates by combining amplified DNA, specific oligonucleotide, and AuNPs. At a temperature of 95 °C, the DNA test undergoes denaturation, resulting in a single-stranded structure. If the oligonucleotide is complementary, it is annealed at 50 °C. The addition of the $MgCl_2$ solution causes instability on the surface of the AuNPs, resulting in particle clustering, a change in the LSRP, and the color turning blue [30]. In contrast, if the oligonucleotide is non-complementary, it will bind to the surface of AuNPs and prevent nanoparticle aggregation in the presence of $MgCl_2$ solution. Thus, the blue spectrum, centered at 548 nm, indicates a positive test with a blue color. However, a negative test exhibits a red color due to oligonucleotide stabilization, which is depicted by the spectrum centered at 537 nm. However, adding $MgCl_2$ solution to all tests can explain the red shift in the LSPS band relative to bare AuNPs (control curve).

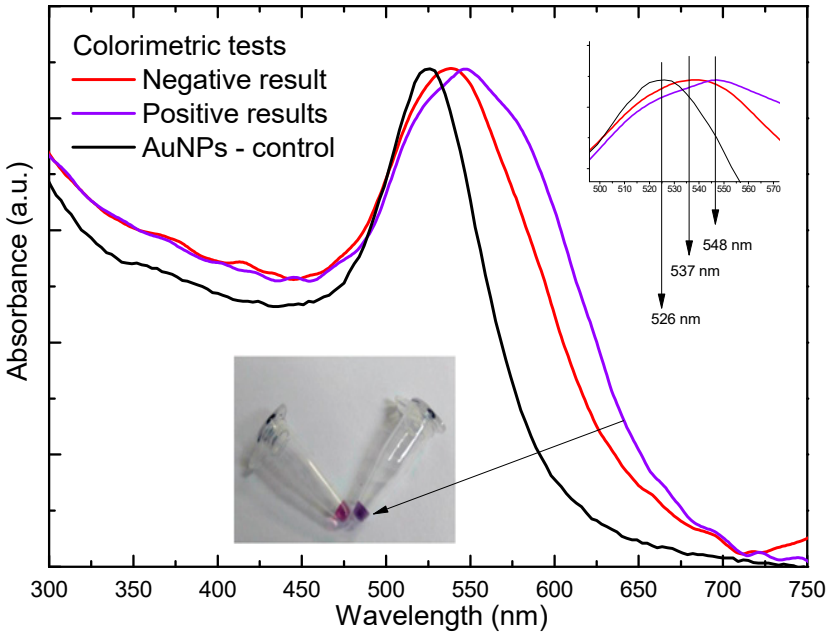

Figure 2. UV–visible spectra of AuNPs from colorimetric tests. The negative result is the red curve, the positive result is the blue curve, and control AuNPs are shown in black.

The most crucial step is to establish a correlation between the results of both positive and negative tests and the observed changes in LSPR in the UV–visible spectra, as shown in Figure 2. Among the fitting curves, the Gaussian function may be used to determine important parameters such as the area under the curve, the curve center, and the Full Width at Half Maximum (FWHM) value. The Gaussian function was fitted in the spectral range of the LSPR, between 450 nm and 650 nm, using the Ftyk Software (version 1.3.1). A box chart summarizing a dataset calculated using Gaussian fitting is shown in Figure 3, highlighting the most significant variation in positive tests.

The box chart shows a red shift at the negative test center location and a broadening in the FWHM. These findings indicate that integrating a specific spectral range would make it possible to distinguish between the tests. Thus, two spectral regions were defined, 488–530 nm and 533–575 nm, respectively, allowing for an automatic validation of the colorimetric test. As shown in Figure 4, Equation (1) successfully separates positive from negative outcomes, with the exception of a false negative result.

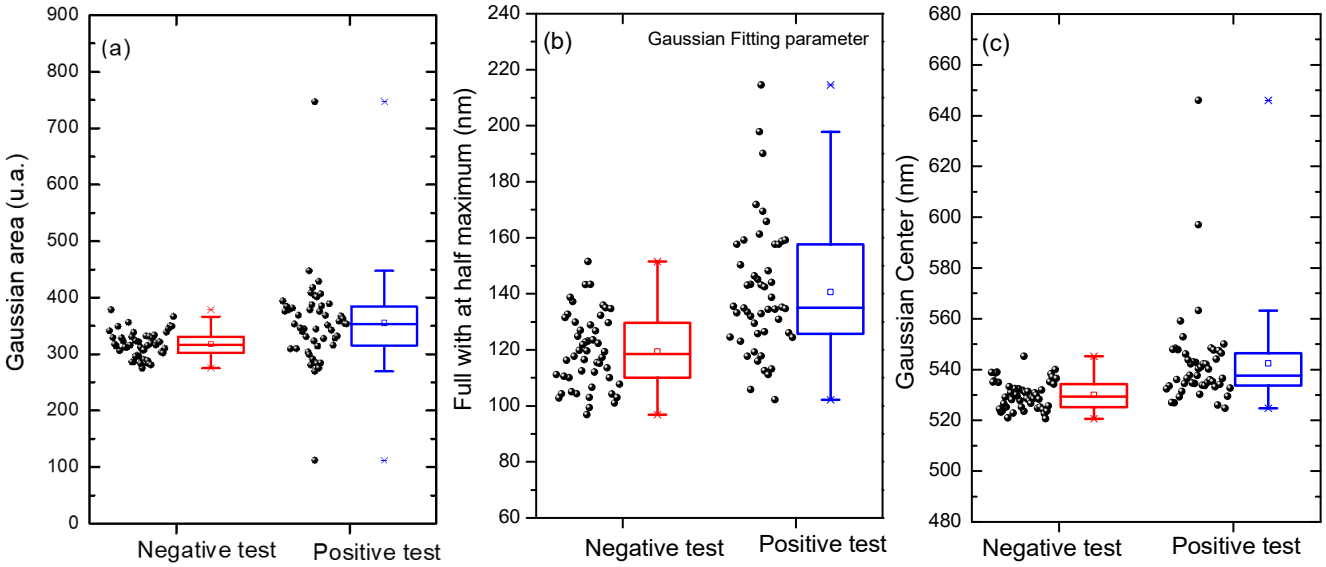

Figure 3. UV–visible spectra of colorimetric test fitted by the Gaussian equation: (**a**) Gaussian area; (**b**) FWHM; (**c**) Gaussian center.

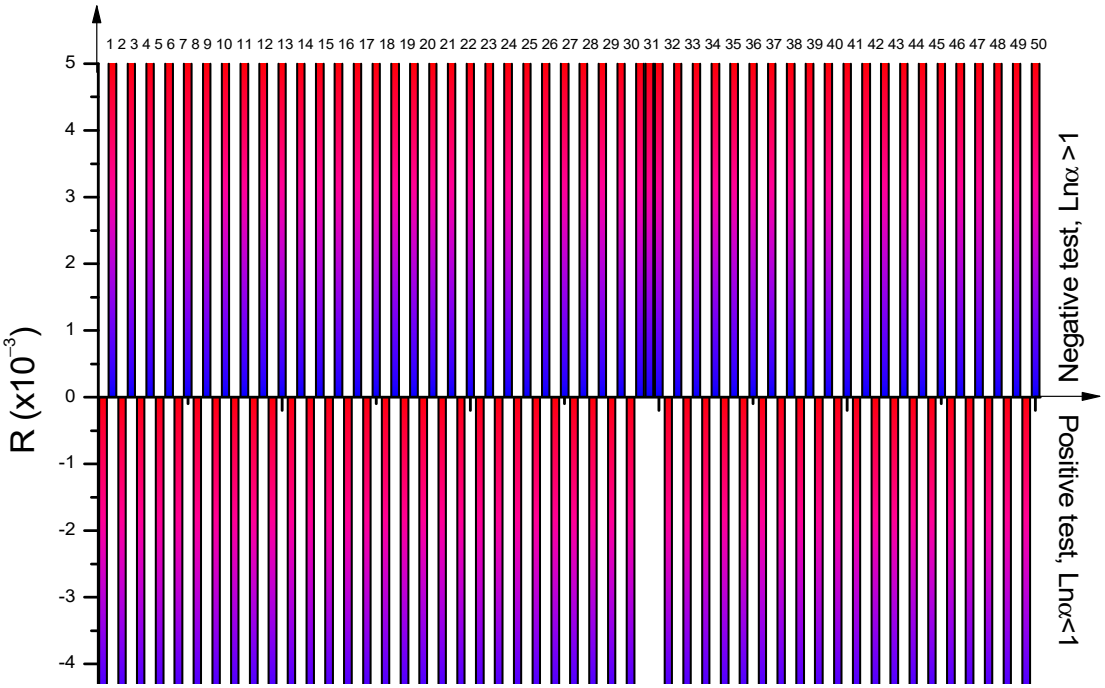

Figure 4. Automatic discrimination of the colorimetric test as determined by Equation (1). The integrated areas of UV–visible spectra were defined by the regions 488–530 nm and 533–575 nm.

In order to certify *P. lutzii* detection by colorimetric testing, a ROC curve was calculated using the classification result obtained from Equation (1). This curve can also be used for multi-class classification, as depicted in Figure 5. The area under the ROC curve represents the overall efficacy of the model and shows 100% sensitivity and 100% specificity.

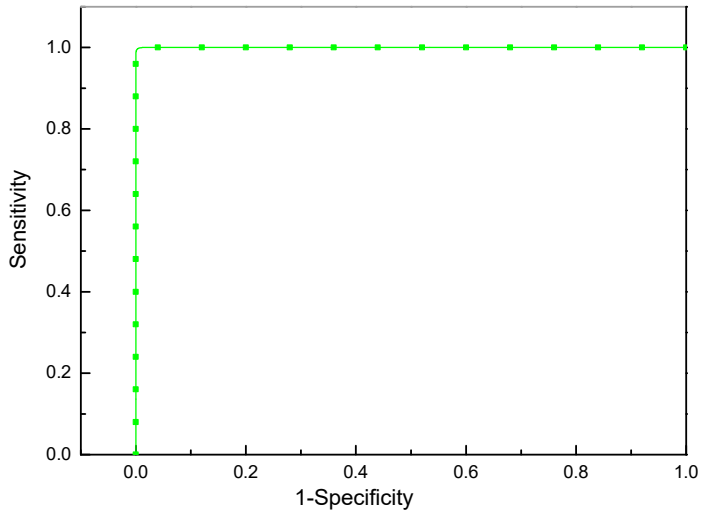

Figure 5. Receiver operating characteristic curve of the colorimetric tests.

4. Discussion

Deforestation disrupts ecosystems, alters wildlife behavior, and facilitates disease transmission. This action is a common occurrence driven by agricultural expansion, urbanization, and infrastructure development [31]. These activities often lead to increased human interaction with ecosystems, potentially exposing individuals to *Paracoccidioides* spp. spores (*P. brasiliensis* and *P. lutzii*) found in the soil, resulting in Paracoccidioidomycosis (PCM) [1]. The overlapping symptoms of PCM can lead to a misdiagnosis as tuberculosis, posing a diagnostic challenge [19–21]. This holds significant importance, as the similarity of symptoms and the absence of glycoprotein Gp43 in *P. lutzii* sometimes lead to the misdiagnosis of PCM.

In this context, a colorimetric test based on colloidal AuNPs associated with PCR products may give successful test results for *P. lutzii* detection. Figure 1 depicts the characteristic AuNPs synthesized by the citrate reduction method, which have a quasi-spherical morphology, an average hydrodynamic diameter of 24 nm, and a zeta potential of −40 mV. The spherical morphology allows for characterization by the DLS technique, which assumes that the particles are spherical and homogeneous, meaning they have a uniform composition and size throughout [32]. This assumption simplifies the mathematical equations used to analyze the data and allows for a straightforward interpretation. The measured zeta potential value shows the good chemical stability of AuNPs against aggregation, which can be explained by an empirical formula [33]. Briefly, the solution is deemed unstable when this value falls within the range of 30 mV to −30 mV, as it exhibits the tendency to self-aggregate over time, making it unsuitable for a colorimetric assay.

The UV–visible spectra also give important information about spherical structure, revealing the presence of a single broad absorption band in the spectra around 526 nm. This phenomenon is related to the LSPR of gold nanoparticles due to the collective oscillation of free electrons on their surface [34]. The UV–visible spectra also allow for the quantification of AuNPs, as described by Navarro et al. [28]. Therefore, the AuNPs can be readily acquired, analyzed, and, importantly, measured using straightforward spectroscopy techniques such as UV–visible spectroscopy, enhancing the test's affordability [35]. Apart from that, AuNPs are excellent candidates for many biomedical applications, such as drug delivery and cancer treatment studies [36–38].

Among the colorimetric test methodologies using colloidal AuNPs, label-free has some advantages compared to cross-linking and non-cross-linking methodologies [24–26,30]. Label-free does not require thiol-oligonucleotides to functionalize nanoparticles by forming self-assembled monolayers on the nanoparticle surface. This process reduces the cost and time of the colorimetric test. The thiol-oligonucleotides need a special column for purification, and the process of immobilizing the oligonucleotides requires several steps to

conjugate the nanoprobes [24]. However, the working mechanism of the colorimetric test is based on changes in LSRP due to a controlled aggregation process. The saline solution is used to cause the AuNPs' aggregation, but when the specific probe does not match a complementary sequence, it finds the stabilization on the AuNPs' surface, preventing self-agglomeration [25,30].

Figure 2 depicts the results of *P. lutzii*'s colorimetric detection, which revealed a color change. To investigate the spectral changes, a Gaussian fit was applied to identify differences in the LSRP band. Figure 3 shows that the positive test produced significant fluctuations, including increased FWHM and area values, as well as a noticeable red shift in the band center. As a result, the ratio of the two spectral regions, combined with Equation (1), was used to automatically validate the colorimetric test shown in Figure 4. Various fields make extensive use of the natural logarithm function, which is especially useful in this context because it displays positive values for negative tests and vice versa. Figure 5 demonstrates that the quantification process produced excellent sensitivity (100%) and specificity (100%).

The most important characteristic of this test is the probe described by 5′ CAG GGG TGC G 3′, which is specific to identifying *P. lutzii* in the amplified molecular region. Even though *P. brasiliensis* and *P. lutzii* have significant genetic similarities with a high degree of genomic conservation and synteny, this indicates their close evolutionary relationship as they belong to the same genus [1]. In addition, colorimetric tests may have highly valuable tools in the diagnosis of diseases in this situation. These tests utilize the genetic information of microorganisms to greatly improve the accuracy of clinical evaluations. It is crucial to emphasize the practical advantages of this method, including its cost effectiveness and user-friendly nature, which make it a promising instrument for healthcare professionals in their everyday work.

5. Conclusions

The synthesized gold nanoparticle had an average size of 24 nm and excellent colloidal stability, which was adequate for the colorimetric test. The detection of *P. lutzii* was achieved using a label-free methodology, revealing important differences between positive and negative tests in UV–visible spectra, such as a red shift at the negative test center location and a broadening in the FWHM. Thus, the integration of two spectral regions was defined: 488–530 nm and 533–575 nm. The ratio between these regions, when combined with the natural logarithm function, gives values of 100% sensitivity and 100% specificity in *P. lutzii* detection. Furthermore, the use of this promising approach in clinical samples could lead to a more accurate diagnosis of PCM through *P. lutzii* detection. This holds significant importance, as the similarity of symptoms and the absence of glycoprotein Gp43 in *P. lutzii* sometimes lead to the misdiagnosis of PCM as tuberculosis.

Author Contributions: Investigation, formal analysis, and methodology, O.O.C.F.; validation and investigation, M.A.C.; writing—original draft preparation, A.V.; investigation and writing—original draft preparation, F.V.M.; writing—original draft preparation and supervision, L.R. All authors have read and agreed to the published version of the manuscript.

Funding: This research was funded by CNPq (302158/2022-7).

Data Availability Statement: The data that support the findings of this study are available from the corresponding author upon reasonable request.

Acknowledgments: Olavo O. Comparato Filho would like to thank CAPES for the PhD scholarship and INMETRO for the TEM analysis.

Conflicts of Interest: The authors declare no conflicts of interest.

References

1. Shikanai-Yasuda, M.A.; Mendes, R.P.; Colombo, A.L.; de Queiroz-Telles, F.; Kono, A.S.G.; Paniago, A.M.M.; Nathan, A.; Valle, A.C.F.D.; Bagagli, E.; Benard, G. Brazilian guidelines for the clinical management of paracoccidioidomycosis. *Rev. Soc. Bras. Med. Trop.* **2017**, *50*, 715–740. [CrossRef] [PubMed]
2. Carvalho, K.C.; Ganiko, L.; Batista, W.L.; Morais, F.V.; Marques, E.R.; Goldman, G.H.; Franco, M.F.; Puccia, R. Virulence of *Paracoccidioides brasiliensis* and gp43 expression in isolates bearing known PbGP43 genotype. *Microbes Infection.* **2005**, *7*, 55–65. [CrossRef] [PubMed]
3. Moura-Campos MC, R.; Gesztesi, J.L.; Vincentini, A.P.; Lopes, J.D.; Camargo, Z.P. Expression and isoforms of gp43 in different strains of *Paracoccidioides brasiliensis*. *J. Med. Vet. Mycol.* **1995**, *33*, 223–227. [CrossRef] [PubMed]
4. Finquelievich, J.L.; Negroni, R.; Iovannitti, C.A.; Elías-Costa, M.R.I. Estudio comparativo de la patogenicidad y la antigenicidad de 6 cepas de *Paracoccidioides brasiliensis*. *Rev. Inst. Med. Trop. São Paulo* **1993**, *35*, 535–541. [CrossRef]
5. Svidzinski, T.I.E.; Miranda Neto, M.H.; Santana, R.G.; Fischman, O.; Colombo, A.L. *Paracoccidioides brasiliensis* isolates obtained from patients with acute and chronic disease exhibit morphological differences after animal passage. *Rev. Inst. Med. Trop. São Paulo* **1999**, *41*, 279–283. [CrossRef] [PubMed]
6. Calcagno, A.M.; Niño-Vega, G.; San-Blas, F.; San-Blas, G. Geographic discrimination of *Paracoccidioides brasiliensis* strains by randomly amplified polymorphic DNA analysis. *J. Clin. Microbiol.* **1998**, *36*, 1733–1736. [CrossRef] [PubMed]
7. Morais, F.V.; Barros, T.F.; Fukada, M.K.; Cisalpino, P.S.; Puccia, R. Polymorphism in the gene coding for the immunodominant antigen gp43 from the pathogenic fungus *Paracoccidioides brasiliensis*. *J. Clin. Microbiol.* **2000**, *38*, 3960–3966. [CrossRef] [PubMed]
8. Feitosa, L.d.S.; Cisalpino, P.S.; dos Santos, M.R.; Mortara, R.A.; Barros, T.F.; Morais, F.V.; Puccia, R.; da Silveira, J.F.; de Camargo, Z.P. Chromosomal polymorphism, syntenic relationships, and ploidy in the pathogenic fungus *Paracoccidioides brasiliensis*. *Fungal Genet. Biol.* **2003**, *39*, 60–69. [CrossRef] [PubMed]
9. Rocha, A.A.; Morais, F.V.; Puccia, R. Polymorphism in the flanking regions of the PbGP43 gene from the human pathogen *Paracoccidioides brasiliensis*: Search for protein binding sequences and poly(A) cleavage sites. *BMC Microbiol.* **2009**, *30*, 277. [CrossRef]
10. Teixeira, M.M.; Theodoro, R.C.; Mendes, F.F.O.; Machado, G.C.; Hahn, R.C.; Bagagli, E.; San-Blas, G.; Felipe, M.S.S. *Paracoccidioides lutzii* sp. nov.: Biological and clinical implications. *Med. Mycol.* **2014**, *52*, 19–28. [CrossRef]
11. Rodrigues, A.M.; Hagen, F.; Puccia, R.; Hahn, R.C.; de Camargo, Z.P. Paracoccidioides and Paracoccidioidomycosis in the 21st Century. *Mycopathologia* **2023**, *188*, 129–133. [CrossRef]
12. Vilela, R.; Huebner, M.; Vilela, C.; Vilela, G.; Pettersen, B.; Oliveira, C.; Mendoza, L. The taxonomy of two uncultivated fungal mammalian pathogens is revealed through phylogeny and population genetic analyses. *Sci. Rep.* **2021**, *11*, 18119. [CrossRef] [PubMed]
13. Turissini, D.A.; Gomez, O.M.; Teixeira, M.M.; McEwen, J.G.; Matute, D.R. Species boundaries in the human pathogen Paracoccidioides. *Fungal Genet. Biol.* **2017**, *106*, 9–25. [CrossRef]
14. Lenhard-Vidal, A.; Assolini, J.P.; Ono, M.A.; Bredt, C.S.; Sano, A.; Itano, E.N. *Paracoccidioides brasiliensis* and *P. lutzii* antigens elicit different serum IgG responses in chronic paracoccidioidomycosis. *Mycopathologia* **2013**, *176*, 345–352. [CrossRef]
15. da Silva, J.F.; de Oliveira, H.C.; Marcos, C.M.; Assato, P.A.; Fusco-Almeida, A.M.; Mendes-Giannini, M.J.S. Advances and challenges in paracoccidioidomycosis serology caused by Paracoccidioides species complex: An update. *Diagn. Microbiol. Infect. Dis.* **2016**, *84*, 87–94. [CrossRef] [PubMed]
16. Peçanha-Pietrobom, P.M.; Tirado-Sánchez, A.; Gonçalves, S.S.; Bonifaz, A.; Colombo, A.L. Diagnosis and Treatment of Pulmonary Coccidioidomycosis and Paracoccidioidomycosis. *J. Fungi* **2023**, *9*, 218. [CrossRef]
17. Puccia, R.; Schenkman, S.; Gorin, P.; Travassos, L.R. Exocellular components of *Paracoccidioides brasiliensis*: Identification of a specific antigen. *Infect. Immun.* **1986**, *53*, 199–206. [CrossRef]
18. de Camargo, Z.P.; Rodrigues, A.M. Paracoccidioides complex. In *Pocket Guide to Mycological Diagnosis*, 1st ed.; Cordeiro, R.D.A., Ed.; CRC Press: Boca Raton, FL, USA, 2020; pp. 125–134.
19. Mayr, A.; Kirchmair, M.; Rainer, J.; Rossi, R.; Kreczy, A.; Tintelnot, K.; Dierich, M.P.; Lass-Flörl, C. Chronic paracoccidioidomycosis in a female patient in Austria. *Eur. J. Clin. Microbiol. Infect. Dis.* **2004**, *23*, 916–919. [CrossRef] [PubMed]
20. Wagner, G.; Moertl, D.; Eckhardt, A.; Sagel, U.; Wrba, F.; Dam, K.; Willinger, B. Chronic Paracoccidioidomycosis with adrenal involvement mimicking tuberculosis—A case report from Austria. *Med. Mycol. Case Rep.* **2016**, *2*, 12–16. [CrossRef]
21. Ekeng, B.E.; Davies, A.A.; Osaigbovo, I.I.; Warris, A.; Oladele, R.O.; Denning, D.W. Pulmonary and Extrapulmonary Manifestations of Fungal Infections Misdiagnosed as Tuberculosis: The Need for Prompt Diagnosis and Management. *J. Fungi* **2022**, *8*, 460. [CrossRef]
22. Leitão, N.P., Jr.; Vallejo, M.C.; Conceição, P.M.; Camargo, Z.P.; Hahn, R.; Puccia, R. *Paracoccidioides lutzii* Plp43 is an active glucanase with partial antigenic identity with *P. brasiliensis* gp43. *PLoS Neglected Trop. Dis.* **2014**, *8*, e3111. [CrossRef] [PubMed]
23. Gegembauer, G.; Araujo, L.M.; Pereira, E.F.; Rodrigues, A.M.; Paniago, A.M.; Hahn, R.C.; de Camargo, Z.P. Serology of paracoccidioidomycosis due to *Paracoccidioides lutzii*. *PLoS Neglected Trop. Dis.* **2014**, *8*, e2986. [CrossRef]
24. Cândido, M.A.; Comparato-Filho, O.O.; Oliveira, I.R.; Castilho, M.L.; Raniero, L. The comparison between label-free and non-cross-linking methods with gold nanoparticles for colorimetric detection of *Paracoccidioides brasiliensis*. *Res. Biomed. Eng.* **2019**, *35*, 39–44. [CrossRef]

25. Storhoff, J.J.; Lazarides, A.A.; Mucic, R.C.; Mirkin, C.A.; Letsinger, R.L.; Schatz, G.C. What Controls the Optical Properties of DNA-Linked Gold Nanoparticle Assemblies? *J. Am. Chem. Soc.* **2000**, *122*, 4640–4650. [CrossRef]
26. Castilho, M.L.; Vieira, L.S.; Campos AP, C.; Achete, C.A.; Cardoso MA, G.; Raniero, L. The efficiency analysis of gold nanoprobes by FT-IR spectroscopy applied to the non-cross-linking colorimetric detection of *Paracoccidioides brasiliensis*. *Sens. Actuators B Chem.* **2015**, *215*, 258–265. [CrossRef]
27. Turkevich, J.; Stevenson, P.C.; Hillier, J. A study of the nucleation and growth processes in the synthesis of colloidal gold. *Discuss. Faraday Soc.* **1951**, *11*, 55. [CrossRef]
28. Navarro JR, G.; Werts MH, V. Resonant light scattering spectroscopy of gold, silver and gold–silver alloy nanoparticles and optical detection in microfluidic channels. *Analyst* **2013**, *138*, 583–592. [CrossRef]
29. Cano, M.I.; Cisalpino, P.S.; Galindo, I.; Ramirez, J.L.; Mortara, R.A.; Silveira, J.F. Electrophoretic karyotypes and genome sizing of the pathogenic fungus *Paracoccidioides brasiliensis*. *J. Clin. Microbiol.* **1998**, *36*, 742–747. [CrossRef]
30. Huixiang, L.; Rothberg, L.J. Label-Free Colorimetric Detection of Specific Sequences in Genomic DNA Amplified by the Polymerase Chain Reaction. *J. Am. Chem. Soc.* **2004**, *126*, 10958–10961.
31. Mahon, M.B.; Sack, A.; Aleuy, O.A.; Barbera, C.; Brown, E.; Buelow, H.; Civitello, D.J.; Cohen, J.M.; de Wit, L.A.; Forstchen, M. A meta-analysis on global change drivers and the risk of infectious disease. *Nature* **2024**, *629*, 830–836. [CrossRef]
32. Bhattacharjee, S. DLS and zeta potential—What they are and what they are not? *J. Control. Release* **2016**, *235*, 337–351. [CrossRef]
33. Dickinson, E. Basic principles of colloid science. *J. Chem. Technol. Biotechnol.* **1989**, *45*, 328–329. [CrossRef]
34. Hang, Y.; Wang, A.; Wu, N. Plasmonic silver and gold nanoparticles: Shape- and structure-modulated plasmonic functionality for point-of-caring sensing, bio-imaging and medical therapy. *Chem. Soc. Rev.* **2024**, *53*, 2932–2971. [CrossRef] [PubMed]
35. Daruich De Souza, C.; Ribeiro Nogueira, B.; Rostelato, M.E.C.M. Review of the methodologies used in the synthesis gold nanoparticles by chemical reduction. *J. Alloys Compd.* **2019**, *798*, 714–740. [CrossRef]
36. Kumar, P.P.P.; Lee, M.; Kim, T. Unlocking the Potential of Gold as Nanomedicine in Cancer Immunotherapy. *J. Nanotheranostics* **2024**, *5*, 29–59. [CrossRef]
37. Engels, E.; Lerch, M.; Corde, S.; Tehei, M. Efficacy of 15 nm Gold Nanoparticles for Image-Guided Gliosarcoma Radiotherapy. *J. Nanotheranostics* **2023**, *4*, 480–495. [CrossRef]
38. Kumar, D.; Mutreja, I.; Kaushik, A. Recent Advances in Noble Metal Nanoparticles for Cancer Nanotheranostics. *J. Nanotheranostics* **2023**, *4*, 150–170. [CrossRef]